Sub-Arcsecond Millimeter Imaging of Disks and Envelopes: Probing the Density Structure

Leslie W. Looney[1], Lee G. Mundy[2], and W.J. Welch[3]

[1] Max-Planck-Institut für extraterrestrische Physik, Garching, Germany
[2] University of Maryland, College Park, MD, USA
[3] University of California, Berkeley, CA, USA

Abstract. Sub-arcsecond observations at millimeter wavelengths are providing spectacular images necessary to study directly the circumstellar disks and inner envelopes of young stellar objects. The millimeter data probe the bulk material in the circumstellar environment, complementing the beautiful optical and infrared images of young disk systems being acquired by the VLT and HST. We present an overview of the BIMA millimeter sub-arcsecond survey of deeply embedded and T Tauri systems, focusing on the morphology of the structures, the inner density in the envelope, and the youngest disks.

1 Introduction

Over the last few decades a general picture of isolated star formation as been realized. Protostars are formed deep within molecular cloud cores, which not only provide the raw materials for star formation, but also influence the evolution and eventual outcome of the system. These young stellar systems are initiated via the collapse of the core, which forms the circumstellar envelope of the protostar. Standard collapse solutions of the singular isothermal sphere [1–4] predict a density structure of $\rho \propto r^{-2}$ that evolves into a $\rho \propto r^{-3/2}$. As the collapse proceeds, a small circumstellar disk forms around the young protostar, growing larger and more massive as the envelope dissipates.

These forming stellar systems exhibit excess infrared and millimeter emission that arises primarily from the two circumstellar dust structures: envelopes and disks. We have completed a millimeter interferometric survey of the youngest, deeply embedded protostars, the so-called Class 0 sources, as well as the older, more evolved Class I/II sources, resolving the disks and the envelopes. In this paper, we will discuss the structures and density of the envelope and their implication in the star formation process.

2 The BIMA Sub-Arcsecond Survey

We have observed 24 young stellar objects [5] in 11 fields using the BIMA millimeter array [6] in the $\lambda = 2.7$ mm continuum. These multi-configuration observations utilized the high dynamic u,v range of the BIMA array: fully sampled spatial scales ranging from $0''.4$ to $60''$. This unique feature of BIMA allows the first consistent comparison of dust emission structures in a variety of systems [5]. The images show a diversity of structure and complexity. The youngest systems are the deeply embedded sources (L1448 IRS3, NGC1333 IRAS2, NGC1333 IRAS4, VLA 1623, and IRAS 16293-2422) which have continuum emission dominated ($\geq$ 85%) by the extended envelope, typical mass of 1 $M_{\odot}$(See Fig. 1). The

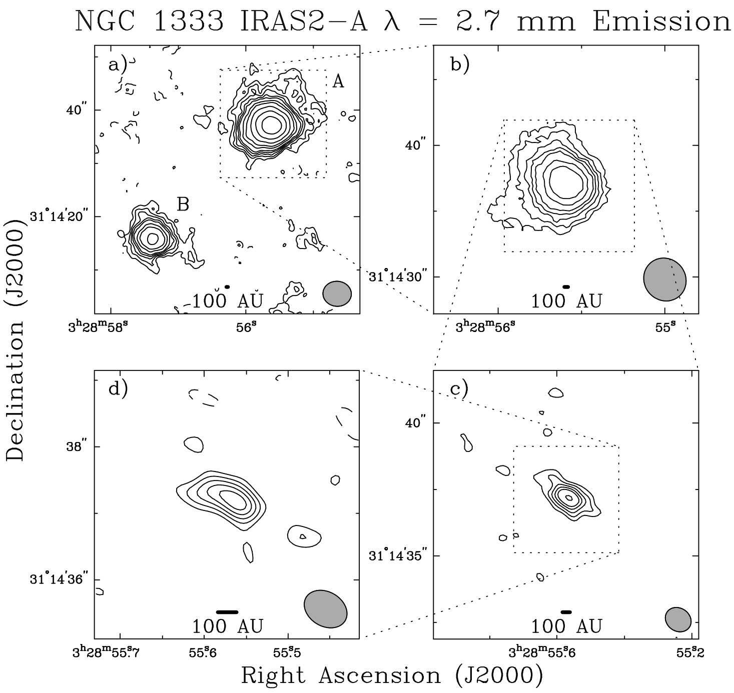

Fig. 1. NGC 1333 IRAS 2 A maps of the λ = 2.7 mm continuum emission. Panel (a) is contoured in steps of (-4 -3 -2 2 3 4 5 6 8 10 14.14 20 28.28 40 56.56) $\times$ the rms of panel (a) of 1.3 mJy/beam. Panels (b) through (d) use a rms noise of 2.7 mJy/beam. (a) σ = 1.3 mJy/beam; beam is $5''.40 \times 4''.70$ P.A. = 86 $^\circ$ (b) σ = 1.2 mJy/beam; beam is $3''.36 \times 3''.16$ P.A. = 45 $^\circ$ (c) σ = 1.7 mJy/beam; beam is $1''.02 \times 0''.87$ P.A. = 57 $^\circ$ (d) σ = 2.7 mJy/beam; beam is $0''.69 \times 0''.52$ P.A. = 60 $^\circ$. Note how the emission is resolved away in higher resolution.

older, less embedded systems which are detected in the near-infrared (SVS13 and L1551 IRS5) have continuum emission that is both extended and compact. The oldest systems in our survey are the optically visible T Tauri stars (DG Tauri, HL Tauri, GG Tauri, and GM Aurigae), which have continuum emission dominated by compact ($\leq$ 1$''$) circumstellar disks, typical mass of 0.02 $M_{\odot}$(See Fig. 2).

All of the surveyed embedded objects are in multiple systems with separations on scales of $\sim$ 30$''$ or less. Based on the system separation, we place the

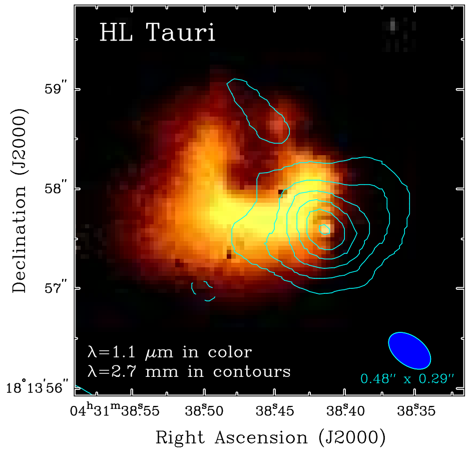

Fig. 2. BIMA sub-arcsecond imaging of the circumstellar disk around HL Tauri in contours [5]; in color is the HST near-infrared image of the reflection nebula [7]. The contours are in steps of (-4 -2 2 4 6 8 10 12) $\times$ 4 mJy/beam. With a beam size of 0.″48 $\times$ 0.″29, the disk is clearly resolved.

objects into three categories: separate envelope (separation $\geq$ 6500 AU), common envelope (separation 150-3000 AU), and common disk (separation $\leq$ 100 AU)[5]. These three groups can be linked with fragmentation events during the star formation process: separate envelopes from prompt initial fragmentation and the separate collapse of a loosely condensed cloud, common envelopes from fragmentation of a moderately centrally condensed spherical system, and common disk from fragmentation of a high angular momentum circumstellar disk.

3 Envelope Modeling

We have performed extensive modeling of the inner envelope structure in many of the deeply embedded sources in our general survey [8]. Our main goal in the modeling is to address two main questions: (1) Can we constrain the power-law of the density to either a $\rho \propto r^{-2}$ or $\rho \propto r^{-3/2}$? (2) What mass constraints can we place on the circumstellar disks in these systems?

To compare the observations directly to models of the dust structure, we have to simplify the models by making assumptions about the dust properties and source morphology. Our source model for the embedded sources is comprised of a spherical dust envelope with an embedded point source meant to represent an unresolved disk. Since the embedded systems in our survey [5] have spherical symmetry, we assume spherical envelopes. In addition, we use a power-law for the density structure, as suggested by solutions of the singular isolated sphere collapse solutions e.g. [1–4].

We adopt the temperature profile model of Wolfire and Cassinelli [9], which self-consistently solves for the temperature throughout the envelope. Past modeling of envelopes have used the simple power-law temperature distribution of optical thin dust. However, for somewhat massive envelopes or steep density power-law indices, the envelope can become optically thick at radii < 200 AU [8], a spatial scale at which our survey is sensitive. We also use a modified version of the MRN [10] and the Draine & Lee [11] optical constants to describe grain properties. Studies have suggested that dust in circumstellar disks and dense cores has a λ^{-1} dependence at submillimeter wavelengths [12–14] rather than the λ^{-2} dependence. Our hybrid model preserves the optical and infrared properties of the MRN dust grain model, while forcing the long wavelength λ^{-1} behavior and $\kappa_\nu(2.7\ \mathrm{mm}) = 0.009\ \mathrm{cm}^2\ \mathrm{g}^{-1}$.

With these assumptions, the model parameters are the inner and outer radii of the envelope, the mass of the envelope, the power-law indices of the density, and the flux of the embedded circumstellar disk. The interferometric data are binned in u,v annuli around the source location and averaged vectorially (see Fig. 3). For the six sources modeled, we fit density power-laws of p = 1.5 and p = 2.0. The other parameters are explored over grids of parameter space: inner radii of 10, 30, 50 and 100 AU, outer radius from 1000 AU to 10000 AU, and a central point source flux in steps starting at no point source, up to a maximum of the amplitude in the last u,v distance bin. The models were treated in the exact same method as the observational data. For each model, the χ^2 was minimized with respect to the envelope mass to produce the best fit to the data.

All six of the sources can be fit with a density power-law index of p = 2.0; in half of the systems, those with the highest signal to noise ratios, p = 1.5 power-law models can be rejected with a $> 95\%$ confidence level. What do these fits tell us about the nature of density structure in the systems? In order to understand the constraints that higher signal to noise systems place on descriptions of the envelope collapse, it is instructive to examine the Larson-Penston (LP) and Shu solutions in more detail.

3.1 Modeling Discussion

In the Shu model, an expansion wave travels from the inner region outwards, the "inside-out" collapse. The head of the expansion wave is roughly where the $\rho \sim r^{-2}$ region transitions to the $\rho \sim r^{-3/2}$ region, and is only dependent upon the time after the formation of the core and the local sound speed. Thus, for a sound speed, a = 0.2 km/s, the head of the expansion wave will be located at 400 and 4000 AU for ages of 10^4 and 10^5 yrs, respectively.

In the LP solution, there is no expansion wave since the initial velocity profile is already collapsing, not at rest as in the Shu solution. Nonetheless, there is an infall scale for the interface between the $\rho \sim r^{-2}$ and $\rho \sim r^{-3/2}$ regions. Since the LP infall velocity is 3.3 times that in the Shu solution, the effective spatial scale is 3.3 times as large. Thus, the radius at which one expects a p = 1.5 is $\sim$ 1300 and 13000 AU for ages of 10^4 and 10^5 yrs, respectively. The larger mass infall rate creates a higher density envelope; the mass of the envelope at the onset of the core formation is 4.4 times larger than in the Shu solution.

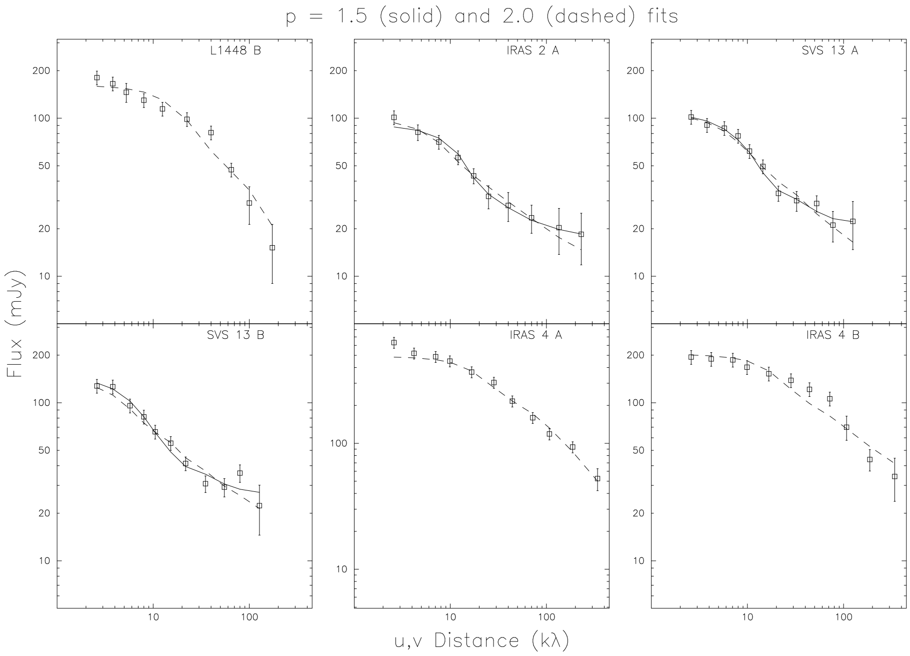

Fig. 3. Model fits for power-law density indices of p=1.5 and p=2.0 presented in u,v space, the separation of antennas. The data are effectively the Fourier transform of the sky brightness distribution. The error bars are statistical error bars based on the standard deviation of the mean of the data points in the bin with a minimum of 10%, reflecting the uncertainty in the overall calibration. For IRAS 4 A, the first data point was not used in the modeling, since it most probably traces larger scale emission that is not part of the inner envelope.

To match the $\rho \sim r^{-2}$ power-law fits, the infall regions in these models must not dominate the radial density profiles. This means that they must be young, which is consistent with their classification as Class 0 sources. The youthfulness of the systems is also supported by the dynamical age estimates for the outflows. For example, L1448 IRS3 has the largest outflow, 14.5′ [15]. For an assumed jet speed of $\sim$ 200 km/s, the minimum age of L1448 IRS3 is $\sim$ 6,200 yrs. The corresponding times for the other systems are shorter, but it must be stressed that these are minimum ages as the outflow region should propagate out at a fraction of the basic jet speed. On the other hand, the luminosity of the system can also constrain the minimum age. In the above example of L1448 IRS3, which has a luminosity of 6.8 $L_{\odot}$, the Shu model for that age would require an increase of sound speed by 75%. For the LP solution, this is less of a problem since the mass accretion is nearly 46.9 times larger.

We have performed more complicated modeling of the sources using the LP and Shu solutions directly. We find that they predict similar ages, since the Shu model requires much larger sound speeds to match the density. In these cases, however, the Shu solution can still not match the luminosity. In our modeling, the LP solution provides a better match to the data, but neither solution is the ideal fit. This is not surprising since numerous computational studies of the isothermal collapse have shown that there is no strong tendency to assume a self-similar form (c.f. [4,16]). Indeed, the computational simulations of the collapse of isothermal spheres demonstrates that it is incorrect to think of the envelopes of young stars as the realization of either collapse model. The truth is likely to be between the two solutions, and our modeling substantiates this.

Finally, one of the primary strengths of this study is the ability of the interferometer to separate large scale emission from compact emission, allowing us to probe for the youngest circumstellar disks embedded within the envelope. In our modeling, all systems have acceptable models with no central point source, but typically, point source flux values are in the range of 0 to 40 mJy.

We can make a mass estimate for the embedded disk using the circumstellar disk of HL Tauri as a standard. A HL Tauri type disk (disk mass ~ 0.05 $M_{\odot}$[5]) has a flux of $\sim$ 100 mJy at the distance of Taurus (140 pc). If placed at the distance of Perseus (350 pc), the flux of HL Tauri would be 16 mJy. So the range of acceptable point source fluxes would represent circumstellar disk masses of 0 to 0.12 $M_{\odot}$. This is a small fraction of the circumstellar envelope mass, typically ~ 1 $M_{\odot}$. In other words, since we do not see disks that are over-massive when compared to the Class I/II systems, there is not a large mass reservoir and as the system evolves from the deeply embedded stage to the more disk dominated stage, the disk must efficiency process material onto the protostar.

References

1. Larson, R.B. 1969, MNRAS, 145, 271
2. Penston, M.V. 1969, MNRAS, 144, 425
3. Shu, F.H. 1977, ApJ, 214, 488
4. Hunter, C. 1977, ApJ, 218, 834
5. Looney, L.W., Mundy, L.G., & Welch, W.J. 2000, ApJ, 529, 477
6. Welch, W.J. et al. 1999, PASP, 108, 93
7. Stapelfeldt, K.R., et al. 1995, ApJ, 449, 888
8. Looney, L.W., Mundy, L.G., & Welch, W.J. 2002, in preparation
9. Wolfire, M.G., & Cassinelli, J.P. 1986, ApJ, 310, 207
10. Mathis, J.S., Rumpl, W., & Nordsieck, K.H. 1977, ApJ, 217, 425
11. Draine, B.T., & Lee, H.M. 1994, ApJ, 285, 89
12. Beckwith, S.V.W., & Sargent, A.I. 1991, ApJ, 381, 250
13. Beckwith, S.V.W. et al. 1986, ApJ, 309, 755
14. Weintraub, D.A., Sandell, G., & Duncan, W.D. 1989, ApJ, 340, L69
15. Bally, J., Devine, D., Alten, V., Sutherland, R.S. 1997, ApJ, 478, 603
16. Foster, P.N. & Chevalier, R.A. 1993, ApJ, 416, 303